



Edge plasma diagnostics on W7-AS and ASDEX-Upgrade using fast Li beams

S. Fiedler^{a,*}, R. Brandenburg^b, J. Baldzuhn^a, K. McCormick^a, F. Aumayr^b,
J. Schweinzer^a, H.P. Winter^b, W7-AS and ASDEX-Upgrade team^{a,b}

^a Max-Planck-Institut für Plasmaphysik, EURATOM Association, D-85748 Garching, Germany

^b Institut für Allgemeine Physik, TU-Wien, Ass. EURATOM-OEAW, A-1040 Vienna, Austria

Abstract

Knowledge of the impurity concentration and temperature in the core plasma gradient region as well as the SOL is a vital element on the road to documenting and understanding the physics of L- and H-mode transport and the transport barrier itself. To this end, the Li-beam diagnostic capabilities on W7-AS and ASDEX-Upgrade have been expanded to include the measurement of radial profiles of impurity ion density and temperature via charge-exchange-spectroscopy (Li-CXS). After presenting the method of Li-CXS this paper describes the experimental setup on W7-AS as well as ASDEX-Upgrade and presents first results on both experiments. Measurements of C⁶⁺ and Ne¹⁰⁺ spectral lines prove the viability of Li-CXS. In the plasma edge region of W7-AS ($r_{\text{eff}} > 8$ cm) a C⁶⁺ concentration of about 0.5% could be measured. Temperature values found for C⁶⁺ are similar to proton/deuteron temperatures. The intensities of several LiI spectral lines (2p→2s, 3d→2p, 4s→2p, 4d→2p) have been measured and are used to critically check the underlying cross section database employed within the collisional-excitation Li-beam model, especially for collision processes involving higher Li-states ($n \geq 3$). It was found that the ratio of the spectral lines corresponding to 3d→2p and 2p→2s transitions is overestimated by the model. These deviations could be eliminated by using improved cross sections in the database. © 1999 Elsevier science B.V. All rights reserved.

Keywords: Beam probe spectroscopy; Carbon impurities; Carbon ions; CCD camera; Charge-exchange recombination; Impurity transport; Ion temperature; Neon; Spectroscopy; Stellarator; W7-AS

1. Introduction

Li-beam diagnostics are a multi-purpose technique for investigating fusion edge plasmas. While the determination of electron densities by lithium impact excitation spectroscopy (Li-IXS) has already reached a satisfactory standard on both large fusion experiments at IPP Garching [1,2], neutral Li-beams can also be used to determine local concentrations as well as temperatures of impurity ions via charge exchange spectroscopy (Li-CXS) [3,4]. This method has been proposed by Winter [5] and was applied for the first time at the TEXTOR tokamak at KFA Jülich [6,7]. In order to

achieve simultaneous Li-IXS and Li-CXS measurements, the setup for electron density measurements has been extended. First results prove the feasibility of Li-CXS with the improved Li-injector [1] in W7-AS plasmas.

2. Principles

From observation of the resonant line radiation profile of the injected Li-beam it is possible to deduce the electron density profile as well as the local Li(nl) state distribution along the injected Li-beam by modeling the Li-beam-plasma interaction. In addition to the impact excitation process the weakly bound outer electron of the Li-atom can also be captured by impurity ions. This charge-exchange process populates highly

* Corresponding author.: e-mail: fiedler@ipp.mpg.de

excited states of the impurity ions, giving subsequently rise to characteristic impurity line radiation. Observation of this line emission in conjunction with the calculated Li(nI) state distribution allows for evaluation of the impurity density profile along the injected Li-beam. In addition, the temperature profile of the impurity ions is determined from the spectral line shape.

3. Experimental setup on W7-AS

The existing Li-beam diagnostic layout [1] has been supplemented by a 14 channel observation system with a radial resolution of $\delta r \sim 6$ mm for a range of ~ 13 cm along the beam, corresponding to an effective plasma radius from 3 to 17 cm, cf. Fig. 1. Two glass lenses ($\Omega/4\pi \sim 2.9 \times 10^{-4}$ sr) image the light onto 14 bundles, each consisting of a 2×4 array of $400 \mu\text{m}$ quartz fibers. The bundles are coupled one by one to the entrance slit of a monochromator (ACTON, Czerny-Turner, $f=0.75$ m) to permit spectral resolution for Li-CXS and LiI radiation. A two-dimensional detector (Proscan CCD camera, 512×512 pixels, each $19 \times 19 \mu\text{m}^2$) is directly connected to the monochromator exit. The spectral resolution can reach up to 0.018 nm/pixel, using a 1800 g/mm grating. An additional system of R928 or R3896 Hamamatsu photomultipliers in conjunction with interference filters ($\lambda=529.0$ nm for C^{6+} , $\text{FWHM} \leq 0.5$ nm) can be coupled to the same light guides for simultaneous measurements at the 14 radial locations.

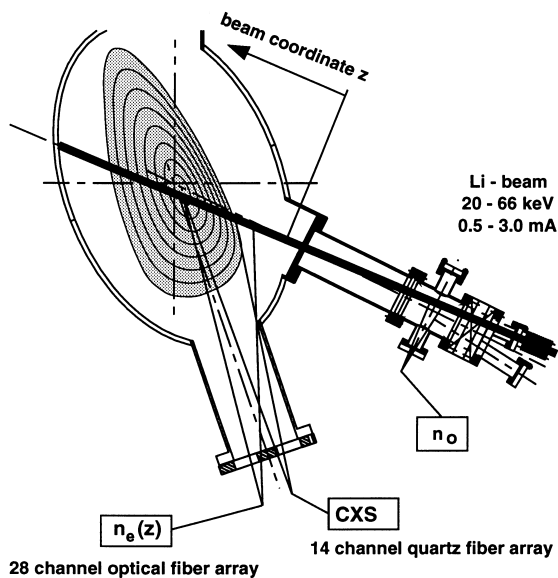


Fig. 1. Experimental set-up on the W7-AS stellarator. The observation geometry for Li-IXS (28 channels), Li-CXS (14 channels) and neutral density n_o is indicated.

The extraction geometry of the Li-beam injector was changed to increase the Li-beam current delivered by the gun [1]. These experiments were carried out at 50 keV injection energy with an equivalent neutral Li-beam current of 1.9 mA and a Li-beam diameter of $D_{\text{FWHM}} \leq 1$ cm.

4. Experimental setup on ASDEX-Upgrade

On the ASDEX-Upgrade tokamak the Lithium beam diagnostics has a new location 33 cm above midplane. It is equipped with a completely rebuilt 35 channel optics to measure electron density profiles, a 16 channel charge exchange optics and a 3 channel neutral density monitoring system (Fig. 2). At the new position of the ion gun, which is similar to the one on W7-AS, the magnetic field is weaker. There is also additional μ -metal shielding around the ion beam. Thus, we expect magnetic field effects on the lithium beam ($E=35$ keV, $I=1.2$ mA) to be reduced considerably.

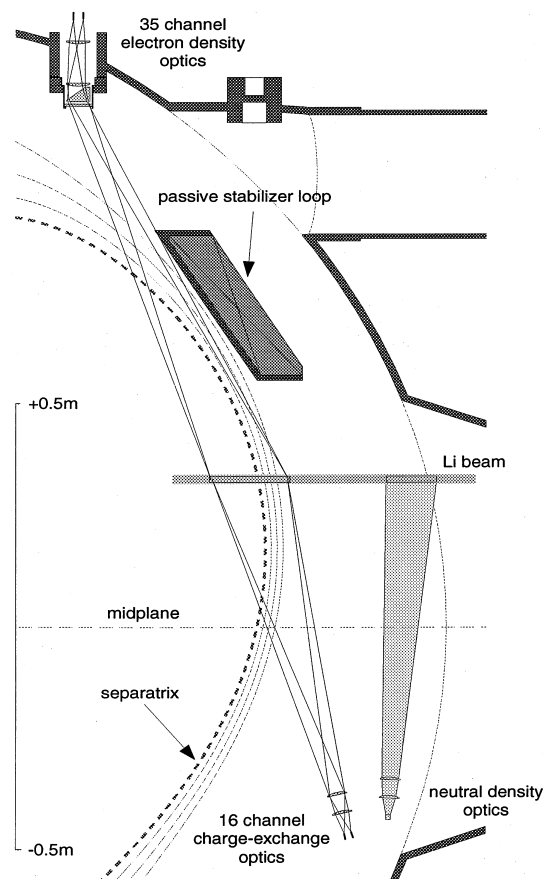


Fig. 2. Optical observation systems of extended lithium beam diagnostics on ASDEX-Upgrade.

4.1. Electron density measurement setup

In the former optical system each spatial channel consisted of three 400 μm fibers. The light collection/transmission efficiency varied drastically from fiber to fiber and the system was sensitive to the beam position [8]. To overcome these difficulties, a new head for the fiberguides was built with each spatial channel corresponding to a bundle of 35 quartz fibers (100/130 μm). The light from each bundle is coupled to a 48 m long, 600 μm monofiber (numerical aperture = 0.37) that carries the light to the detection units. About seven percent of the incoming light can be collected in this way. A new BK7 optical system – a wedge and two lenses – was built to gather light into 35 channels from about 16 cm along the beam path. The observation region can be radially shifted by a couple of centimeters, allowing it to be adjusted to different plasma scenarios. Each detection unit is equipped with an interference filter ($T > 40\%$, $\text{FWHM} \leq 0.7 \text{ nm}$) followed by a photomultiplier.

4.2. CXS measurement setup

Two quartz lenses ($\Omega/4\pi \sim 1.5 \times 10^{-3} \text{ sr}$) focus the light onto an array of 16 quartz fibers (400 μm) enabling the radial distribution of the emitted light in a 16 cm region around the separatrix to be measured with 1 cm spatial resolution. The fibers are coupled to the entrance slit of the same CXS spectroscopic system as described for W7-AS. Temporal resolution is limited by the read-out time of the CCD detector for 16 channels (13 ms).

4.3. Neutral density measurement setup

Two BK7 lenses ($\Omega/4\pi \sim 1.8 \times 10^{-3} \text{ sr}$) focus the light onto an array of 21 quartz fibers (400 μm) that are grouped into three bundles. The light is gathered from a region far from the separatrix where lithium excitation by collision with neutrals is the dominant process [2]. Each channel is equipped with an interference filter ($T > 40\%$, $\text{FWHM} \leq 0.7 \text{ nm}$) to select the $\text{Li}(2p \rightarrow 2s)$ line.

5. Lithium beam composition

Since the cross sections for charge exchange processes from the Li donor atom into excited states of various plasma impurities depend strongly on the originating $\text{Li}(nl)$ states, the composition of the Li-beam is of great importance for evaluating CXS data. We have therefore investigated several LiI spectral lines ($2p \rightarrow 2s$, $3d \rightarrow 2p$, $4s \rightarrow 2p$, $4d \rightarrow 2p$) in W7-AS and ASDEX-Upgrade discharges.

While the measurements of the most relevant line $\text{Li}(2p \rightarrow 2s)$ at $\lambda = 670.8 \text{ nm}$ were performed to calibrate the CXS setup relative to the Li-IXS photomultiplier

setup (see below), all other LiI lines were investigated to check the attenuation model of the Li-beam [9]. In a first approach on W7-AS, measured intensities of emission from higher levels were found to differ considerably (30–60%) from corresponding theoretical values. We observed no dependence on magnetic field strength and beam energy (20–66 keV). The plasma density had a strong influence on the conformity of experimental and theoretical values, with the deviation becoming larger at higher densities.

As the major reason for these disagreements, inadequate scaling relations for excitation and ionisation processes involving electrons and protons in the underlying database [10] were identified. These have now been measured and recalculated by more advanced means and have been found to be considerably lower than the (scaled) cross sections used so far (cf. Fig. 3).

When comparing experimental values of relative $\text{Li}(nl)$ population numbers with results from the improved beam modelling, an excellent agreement can be stated (Fig. 4).

However, since the relative population of the $\text{Li}(3d)$ state in the Li-beam is in the range of 1%, and populations of all other $\text{Li}(nl)$ levels ($n > 2$) are even smaller, the influences of these new cross sections on electron density calculations remain below 10% (cf. Fig. 5).

6. CXS investigations on W7-AS

6.1. Impurity density profiles

To determine the absolute concentration of C^{6+} impurity ions, both Li-beam diagnostic systems are nec-

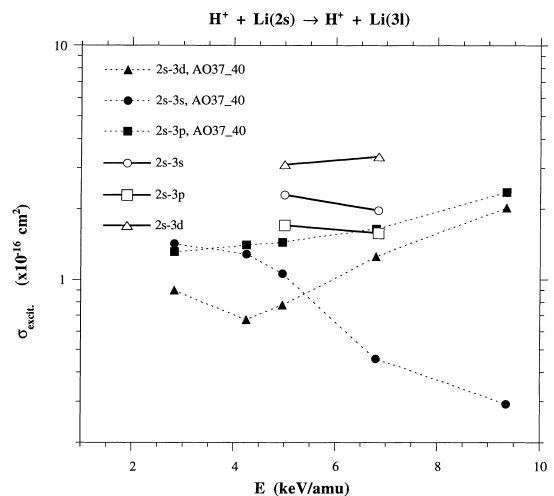


Fig. 3. Comparison of proton impact excitation cross sections from the current database [10] with recent atomic orbital – close coupling calculations (AO37_40). Calculated values are significantly lower than scaled values from the database.

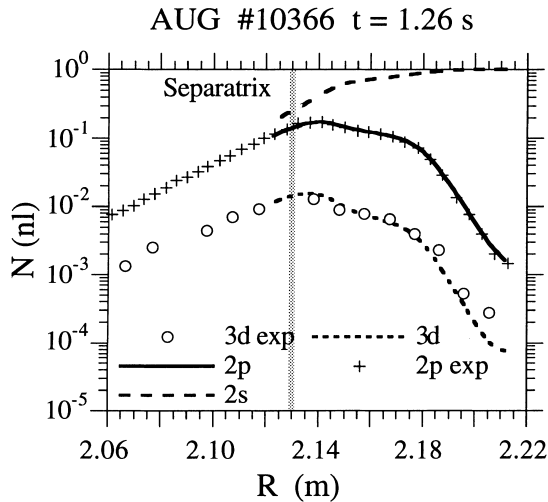


Fig. 4. Radial profiles of relative Li(*nl*) populations when the Li beam penetrates the plasma edge. Experimental results prove the reliability of the beam modelling when utilising the new cross sections.

essary (IXS and CXS). While the IXS system (28 PM) records the Li(2p) light emission, the CXS system (CCD-camera) delivers the CVI line radiation at 529.0 nm. Since both systems use different observation optics, the detection efficiency has to be cross-calibrated. This is done by measuring the Li(2p) light with both systems, the IXS-PM- ($U_{2p}^{PM}(i)$) and the CXS-CCD-system ($U_{2p}^{CCD}(i)$), respectively in one calibration discharge.

$$U_{2p}^{PM}(i) = k_{671}^{PM}(i) \cdot n_{Li} \cdot A_{2p \rightarrow 2s} \cdot N(2p), \quad (1a)$$

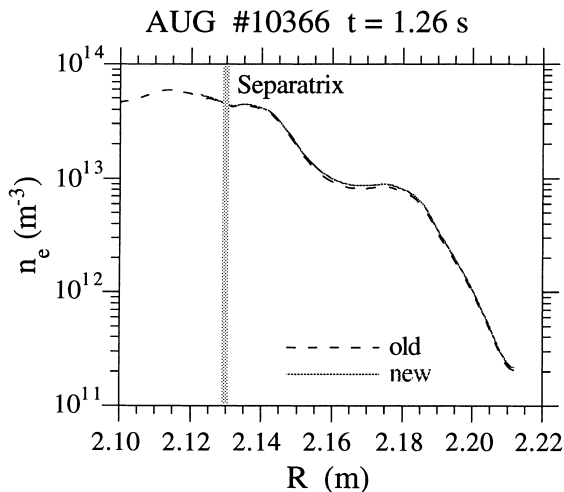


Fig. 5. Comparison of reconstructed electron density profile using 'new' and 'old' cross sections. The influences on the electron density calculations remain below 10%.

$$U_{2p}^{CCD}(i) = k_{671}^{CCD}(i) \cdot n_{Li} \cdot A_{2p \rightarrow 2s} \cdot N(2p), \quad (1b)$$

where k denotes the detection efficiency for the two systems at $\lambda = 671.0$ nm, i the corresponding radial channel, $A_{2p \rightarrow 2s}$ the transition probability, n_{Li} the particle density of the Li-beam and $N(2p)$ the relative occupation number of the 2p-state. The CXS-signal ($U_{529}^{CCD}(i)$) can be expressed by

$$U_{529}^{CCD}(i) = k_{529}^{CCD}(i) \cdot v_{Li} \cdot n_{C^{6+}} \cdot n_{Li} \cdot \sum_{nl} \sigma_{529}(nl) \cdot N(nl). \quad (2)$$

Calculating the ratio of Eqs. (1b) and (2) for the discharges in question and using the ratio of Eqs. (1a) and (1b) for the calibration discharge, the C^{6+} density can be expressed by

$$n_{C^{6+}}(z_{Li}(i)) = \frac{U_{529}^{CCD}(i)}{U_{2p}^{PM}(i)} \cdot \frac{k_{671}^{PM}(i)}{k_{671}^{CCD}(i)} \cdot \frac{k_{671}^{CCD}(i)}{k_{671}^{PM}(i)} \cdot \frac{A_{2p \rightarrow 2s} \cdot N(2p)}{v_{Li} \cdot \sum_{nl} \sigma_{529}(nl) \cdot N(nl)}. \quad (3)$$

In Eq. (3) the first ratio describes the measured signals ratio (IXS and CXS systems), the second ratio is determined by the calibration procedure (see above) and the third ratio expresses the different detection probabilities of the CCD camera at the two wavelengths. v_{Li} denotes the Li-beam particle velocity and $\sigma_{529}(nl)$ the cross section for electron capture from the Li(*nl*)-level, giving rise to line radiation at $\lambda = 529.0$ nm. The relative occupation numbers $N(nl)$ of the Li-beam atoms are calculated in the reconstruction process for the electron density (Li-IXS, [9]). The described algorithm was applied in a series of equivalent discharges ($P_{ECRH} = 400$ kW, D_2 , $l = 0.34$, $B_z = 20.0$ mT, up/down limiters attached, $\int n_e dl$ (HCN) = 2×10^{19} m⁻²) to determine the C^{6+} impurity ion density for different radial positions (different z_{Li} in Eq. (3)). The result is shown in Fig. 6. The C^{6+} impurity ion concentration increases from about 0.41% at $r_{eff} = 16.7$ cm to 0.63% at $r_{eff} = 8.3$ cm. In the gradient region of the profile good agreement is found with the result from the H-CXS diagnostics [11].

For a single light guide in the radial range of the maximum of the Li(2p) profile we also investigated the signal-to-background ratio for other impurity ions. While the ratio was about 0.25 for C^{6+} we found a ratio of 0.2 for C^{5+} and B^{5+} respectively, clearly demonstrating the applicability of Li-CXS also for these impurity ions. The exposure time of the CCD camera was about 5.7 ms with a readout time of 3 ms. Each 10 ms a CCD-picture was recorded. The Li-beam was chopped electronically with a beam on – and off time of 40 ms each. Thus 4 CCD-pictures could be used to determine Li-CXS and background signals. For the determination of impurity densities the Li-CXS signals were summed over the Li-beam on-time interval (40 ms). No impurity

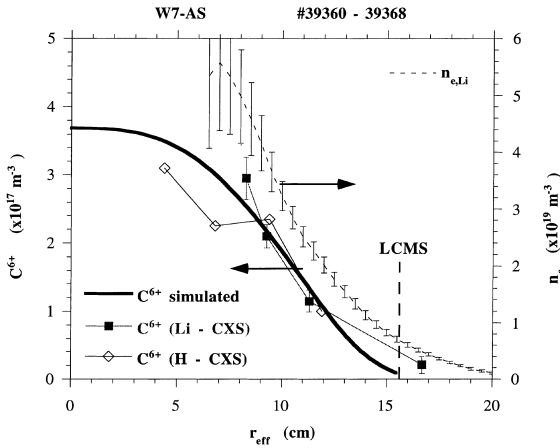


Fig. 6. Radial impurity density profile of C^{6+} and electron density profiles as a function of effective radius r_{eff} for discharges #39360–39368. Thick line shows the result of a simulation with the IONEQ code. The last closed magnetic surface (LCMS) is indicated by a dotted line.

ion concentrations giving rise to CXS-line radiation in the UV-spectral range could be investigated, due to insufficient transmission of the observation optics (glass).

6.2. Simulation of the charge state distribution

The IONEQ code [12] was used to simulate the radial carbon charge state distribution for W7-AS plasmas. Within this simulation the charge state distribution is calculated according to the Corona equilibrium. In addition the impurity transport fluxes are modelled by assuming reasonable values for a diffusion coefficient and a convection velocity. As input data the electron density profile from the Li beam and the temperature profile from the Thomson diagnostics was used. The neutral gas density was modelled by the EIRENE code and calibrated with the H_α and the neutral density measurement of the Li beam diagnostics [13].

A good agreement was achieved with a diffusion coefficient of $D = 0.2(\text{m}^2/\text{s})$

To account for the relatively high displacement of electron and C^{6+} density profiles a strong inward velocity of

$$v_{\text{LCFS}} = -4 \times \frac{D}{r_{\text{LCFS}}} \left[\frac{\text{m}}{\text{s}} \right]$$

with a radial dependency of

$$v(r) = v_{\text{LCFS}} \times \left(\frac{r_{\text{eff}}}{r_{\text{LCFS}}} \right)^2$$

had to be assumed and cannot be explained by uncertainties in the mapping process of local to magnetic coordinates, as the electron and impurity density profiles

are measured at the same toroidal position. Only the electron temperature profile is subject to errors in the radial position of about 0.5 cm. By shifting the T_e profile 1 cm inwards and by the variation of the neutral density profile as well as the diffusion coefficient the influence of these parameters on the radial position of the simulated C^{6+} profile was found to be below a few millimetres (Fig. 6).

6.3. Impurity temperature profiles

Temperature values are obtained by fitting a Gaussian profile to the CCD-camera data. To reduce the scatter of the calculated spectral line widths, all CCD-pictures taken in the flat top phase of one discharge had to be summed up. This typically implies an integration time of about 300–400 ms. The time resolution will be improved by a better coupling of the light guide bundles to the spectrometer entrance slit, where now an important fraction of the light signal is being lost.

For the fitting procedure line broadening effects such as Zeeman splitting and l-level mixing are taken into account [7]. C^{6+} temperature values in the plasma edge obtained in the same series of discharges (see above) are shown in Fig. 7. For $r_{\text{eff}} < 12$ cm C^{6+} temperature values are similar to proton/deuteron temperatures measured via active neutral particle analysis [14].

7. CXS investigations on ASDEX-Upgrade

7.1. Impurity density profiles

On ASDEX-Upgrade we use the spectrometer and CCD camera for investigation of impurity ion spectral

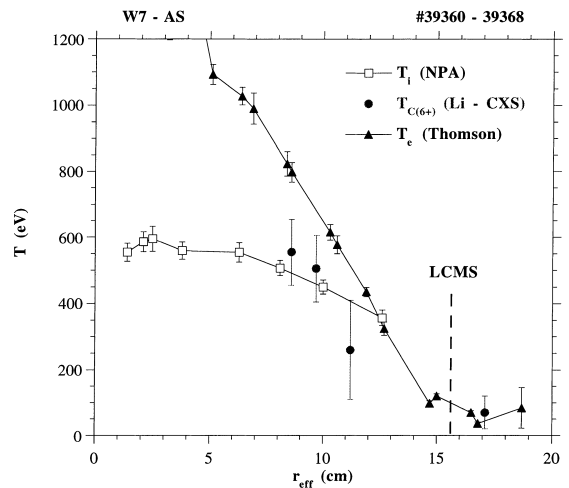


Fig. 7. Radial impurity temperature profiles of C^{6+} , electron temperature T_e and deuterium temperature T_{D^+} measured by neutral particle analysis (NPA) [14].

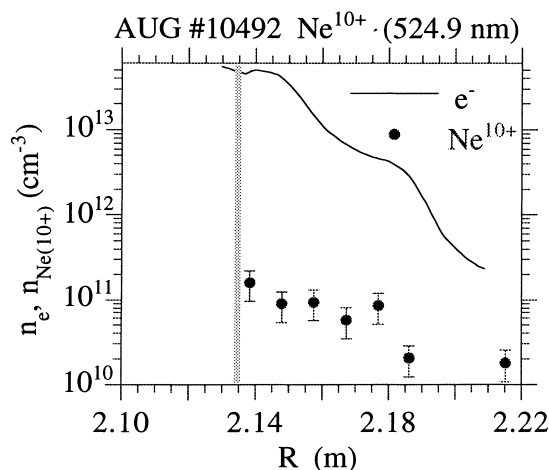


Fig. 8. Profiles of electron and Ne¹⁰⁺ densities in discharge #10492 as a function of major radius R . A strong Ne gas puff occurred during this discharge. Signals have been averaged in the period $2.5 < t < 3$ s.

lines in the range from $250 < \lambda < 800$ nm. The complex temporal behaviour of the ASDEX-Upgrade discharges poses severe difficulties for the Li-CXS method with the current setup. First results indicate the feasibility of Li-CXS for several impurities (Ne⁶⁺, Ne¹⁰⁺, O⁺, He⁺, B²⁺). As an example Fig. 8 shows the profiles of electron and Ne¹⁰⁺ densities as a function of major radius R in a discharge (#10492, $\int n_e d(\text{DCN}) = 8 \times 10^{19} \text{ m}^{-2}$, $I_p = 1$ MA, NI = 5.6 MW) with a strong Ne gas puff.

8. Conclusions

With the improved Li-injector now available we have demonstrated the applicability of Li-CXS, both for impurity density and impurity temperature measurements, on W7-AS. Concentrations found for C⁶⁺ ions are in the order of 0.5%. The radial profile in the gradient region coincides with values from the H^o-CXS-diagnostics. This profile could only be modelled by assuming a strong inwards velocity. Temperature values in the

plasma edge can be considered to be equal to those for deuterium ions. Radial and temporal resolutions of 0.5 cm and 40 ms, respectively (400 ms for temperature measurements) could be achieved. By improving the detection efficiency mainly by using new fibers with smaller aperture and a new construction of the fibers-spectrometer coupling, the temporal resolution can probably be increased by more than a factor of 5. On the ASDEX-Upgrade tokamak the applicability of Li-CXS could be demonstrated by measuring the radial profile of Ne¹⁰⁺ ions.

Acknowledgements

This work has been supported by Friedrich Schiedel-Stiftung für Energietechnik and by Kommission zur Koordination der Kernfusionsforschung at the Austrian Academy of Sciences.

References

- [1] K. McCormick et al., Fusion Eng. Design 34&35 (1997) 125.
- [2] S. Fiedler, IPP Report III/209 (1995).
- [3] E. Wolfrum et al., Rev. Sci. Instrum. 64 (1993) 2285.
- [4] F. Aumayr et al., J. Nucl. Mater. 196–198 (1992) 928.
- [5] H. Winter, Comments Atom. Molec. Phys. 12 (1982) 165.
- [6] R.P. Schorn et al., Appl. Phys. B 52 (1991) 71.
- [7] R.P. Schorn et al., Nucl. Fusion 32 (1992) 351.
- [8] J. Schweinzer et al., in: 22th EPS Conf., Europhys. Conf. Abstr. 19C III (1995) 253.
- [9] J. Schweinzer et al., Plasma Phys. Contr. Fusion 34 (1992) 1173.
- [10] D. Wutte et al., At. Nucl. Dat. Tables 65 (1997) 155.
- [11] J. Baldzuhn et al., Rev. Sci. Instrum. 68 (1997) 1020.
- [12] A. Weller, D. Pasini, A.W. Edwards, R.D. Gill, R. Granetz, JET-IR(87)10.
- [13] S. Fiedler et al., in: 23rd EPS Conf., Europhys. Conf. Abstr. 20C Part III (1996) 1009.
- [14] M. Kick et al., in: 20th EPS Conf., Europhys. Conf. Abstr. 17C Part I (1993) 357.